Monte Carlo Studies for a Neutral Current Based Supernova Neutrino Detector

David M South

THE UNIVERSITY
of MANCHESTER

May 2000

High Energy Group
Department of Physics and Astronomy

First Year PhD Transfer Report

Contents

List of Figures

List of Tables

Abstract

The possibility that μ and τ neutrinos have a non-zero mass is investigated using the neutral current inelastic scattering interaction of neutrinos from supernovae with nuclei. This is the principle behind OMNIS, which detects neutrons produced by this flavour sensitive interaction. In this report I present my work simulating a prototype detector and the processes leading to a detector signal, including a new parameterisation of the Gadolinium decay spectrum to improve the accuracy of the simulation.

Chapter 1

Introduction

When a star reaches the end of its life, if its mass is large enough it will undergo a catastrophic gravitational collapse, resulting in a supernova explosion. The optical emission from these events can outshine the galaxy for many days. This core collapse, which occurs in a matter of seconds, produces a burst of about 10^{58} neutrinos containing particles and antiparticles of all three flavours, in approximately equal numbers. The most famous supernova in our own galaxy occurred in 1054 AD, which created the Crab Nebula, an object still observable today [1]. In 1987, a supernova occurred in the Large Magellanic Cloud, a satellite galaxy of our own and although at a distance of almost 50 kpc, a sufficient number of $\overline{\nu_e}$ events were recorded to demonstrate the viability of the detection of such phenomenon.

Due to obscuration, optical emission from supernovae in our own galaxy is only visible out to about 4 kpc. This region contains only 5% of the stars which end in a suitable Type II or Type Ib, neutrino producing supernova (Figure 1.1). If the visible rate is extrapolated accordingly, an expectation rate of suitable supernovae in the whole galaxy of one every 12-16 years is arrived at. Although this rate is low, these events still provide an opportunity to attempt to unravel the physics of neutrinos.

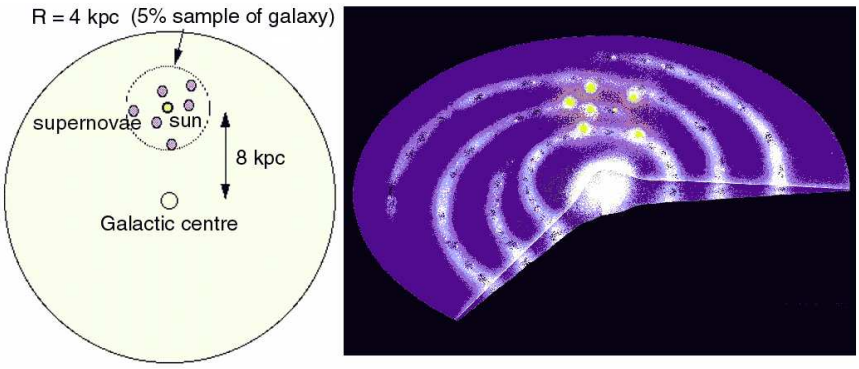

Figure 1.1: The positions of the recorded supernovae in the Milky Way in the past 1000 years. The circled region contains 5% of the stars in the galaxy.

1.1 Neutrino Mass Measurements

The Standard Model predicts the mass of all neutrino flavours to be zero. However, several theories, notably neutrino oscillations, require at least one of the neutrino masses to be non-zero. The contradiction, commonly known as 'The Solar Neutrino Problem', between the Standard Solar Model and the neutrino fluxes measured by experiments such as Kamiokande [2] is explained using such postulates. Oscillations can occur in vacuo or in a medium where a density gradient exists (the MSW effect)[3].

A non-zero neutrino mass also has cosmological significance for the evolution of the universe. The closure parameter, Ω, is defined as follows

$$\Omega = \frac{\rho}{\rho_{crit}} \tag{1.1}$$

where ρ is the current density and ρ_{crit} is the critical density of the universe. Observations of the baryonic universe suggest that $\Omega_{baryonic} \approx 0.1$ and inflation theory requires that $\Omega = 1$, attributing the remainder to non-baryonic matter. Current astrophysical models suggest this remainder is made up of a non-relativistic component, Cold Dark Matter (CDM) and relativistic Hot Dark Matter (HDM). If the sum of the neutrino masses is of order 30 eV, they could account for the HDM component.

To date, no experiment has measured an absolute, non-zero neutrino

Neutrino flavour	Upper mass limit	Confidence level	Ref.
ν_e	m $<$ 2.8 eV	95 %	[4]
ν_μ	m $<$ 170 keV	90 %	[5]
ν_τ	m $<$ 18.2 Mev	95 %	[6]

Table 1.1: Latest upper mass limits on the three neutrino flavours.

mass. The latest results from on going experiments are presented in Table 1.1, which place upper limits on the masses of all three neutrino flavours [4],[5],[6]. Currently active neutrino experiments suffer from being sensitive only to the ν_e (Super Kamiokande [7]) or being insensitive to the neutrino flavour arriving at the earth (SNO [8]).

Our aim is to measure the time profile of ν_μ's and ν_τ's on arrival at the earth produced in a supernova explosion, and hence deduce a limit on their respective masses. Neutrinos incident on the Earth can interact with heavy nuclei to produce neutrons, which may be detected by a suitably designed detector. The inelastic cross section for this interaction is an order of magnitude higher for ν_μ's and ν_τ's than for ν_e's, hence the detector acts as a flavour filter and provides a unique insight into neutrino astro-particle physics [9].

1.2 Project Motivation

Previous Monte Carlo simulations have been written to model neutron transport through different materials and investigate the feasibility of using loaded scintillator as a detector material [9],[10]. This project applies relevant ideas from these works to write a new Monte Carlo simulation for a new detector design.

The modelling of the new detector and steps taken to optimise its geometry are described in Chapter 3. Neutron transport through the various materials is modelled and the number of neutrons detected is estimated. Extensive parameterisation of the spectrum of Gadolinium decays is carried out, to improve the accuracy of the simulation. The number of gammas produced per neutron capture is presented, and the number entering the scintillator

material for detection is calculated. This report assesses the viability of the new detector design and analyses the quality of the new spectrum model.

Chapter 2

Theory

2.1 Neutrinos from Supernovae

A supernova explosion releases approximately 10^{44} J of energy, mostly as a burst of neutrinos that stream isotropically outwards from the supernova. As the core begins to collapse, an initial burst of electron neutrinos occurs due to electron capture on protons:

$$p + e^- \rightarrow n + \nu_e \tag{2.1}$$

This is followed by the main outburst in all three flavours due to thermal pair production. As the core density increases, the neutrinos reach thermal equilibrium and are trapped within the dying star, in a region named the neutrinosphere. However, the increasing pressure gradient causes a 'hydrodynamic bounce' and the neutrinos diffuse away from the core on a timescale of 10-15 seconds. The ν_μ's and the ν_τ's do not undergo charged current interactions, so consequently they suffer fewer collisions and have a higher characteristic temperature compared to that of the ν_e's. Therefore, on arrival at the Earth, the energy of the free ν_μ's and ν_τ's is higher with respect to the energy of the ν_e's.

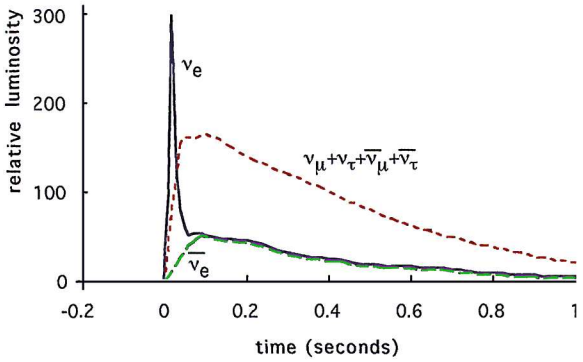

Figure 2.1: Predicted time profile for all three neutrino flavours emitted by a Type II/Ib supernova.

2.2 Mass Measurement of Supernovae Neutrinos

The approximate luminosity time profile of the incident neutrinos is displayed in Figure 2.1 [11]. If the mass of all three types is zero, they will traverse the distance from the supernova to the earth simultaneously, at the speed of light. However, as the neutrino mass increases the time of flight lengthens, so detection of a different luminosity 'rise time' for each flavour would lead to a direct measurement of a limit on the masses. A 'cosmologically significant' neutrino mass in the range 10-100 eV would be directly observable as a delayed component of the time profile. For example, if the ν_τ has a large mass compared to the others, it's arrival time is delayed by

$$\Delta t(s) = 0.5 \left(\frac{R}{10kpc}\right) \left(\frac{m(\nu_\tau)}{20eV/c^2}\right)^2 \left(\frac{20MeV}{E(\nu_\tau)}\right)^2 \tag{2.2}$$

Integrating this delay over the neutrino energy spectrum distorts the time profile for a non-zero mass neutrino, extending the range of arrival times and producing a second peak for masses greater than about 30 eV, as illustrated in Figure 2.2. A significant distortion occurs for masses $m_\nu \geq$ 5-10 eV.

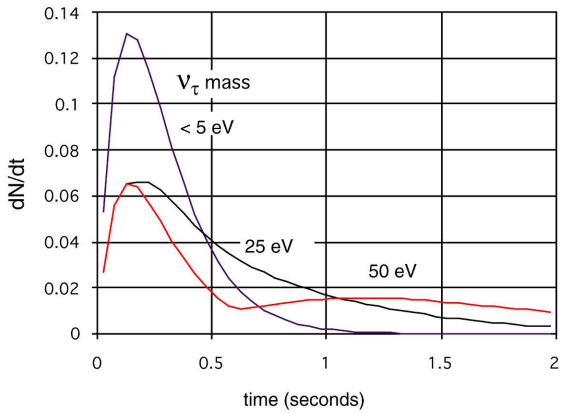

Figure 2.2: The effect of non-zero neutrino mass on the arrival time profile, for a supernova at 8 kpc.

2.3 The Neutrino-Nucleus Interaction

The principle of detection is neutral current scattering. The incident neutrinos may interact with a nucleus via Z^0 exchange, as shown in Figure 2.3. The excited nucleus may then decay via neutron emission:

$$\nu + {}^{A}_{Z}X \rightarrow \nu + {}^{A}_{Z}X^{*} \rightarrow {}^{A-1}_{Z}X + n \tag{2.3}$$

It is the detection of these neutrons, whilst shielding from possible background sources, that is the principle behind OMNIS - **O**bservatory for **M**ulti-flavour **N**eutrino **I**nteractions from **S**upernovae [12].

The excitation cross section for the above interaction increases with incident energy [9]. The flux averaged cross section is given by:

$$\sigma_{FD}(T_\nu) \simeq \sigma_0 \int_0^\infty dE_\nu F_\nu(E_\nu, T_\nu) \int_0^{E_\nu} dE'_\nu E'^2_\nu \beta(\langle E \rangle, E' - E) \tag{2.4}$$

where $F_\nu(E_\nu, T_\nu)$ is the neutrino flux at energy E_ν from the supernova, taken to be a normalised Fermi-Dirac distribution of temperature T_ν with zero chemical potential:

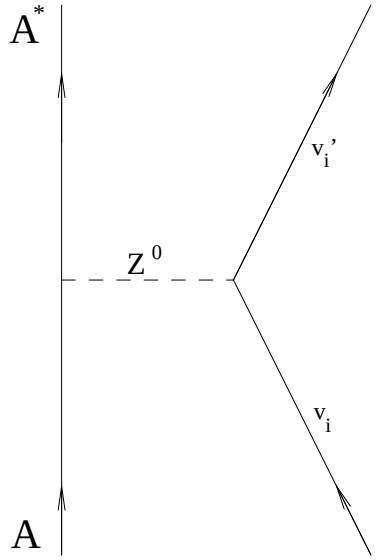

Figure 2.3: The neutrino-nucleus interaction. Nucleus A interacting with a neutrino ν_i via Z^0 exchange.

$$F_\nu(E_\nu, T_\nu) = \frac{0.5546}{T_\nu^3} \times \frac{E^2}{e^{\frac{E}{T_\nu}} + 1} \tag{2.5}$$

and σ_0 is an overall cross section scale factor:

$$\sigma_0 \simeq 2.584 \times 10^{-44} cm^2 MeV^{-2} \tag{2.6}$$

The temperature dependence of the strength function $\beta(\langle E \rangle, E' - E)$ enhances the cross section for higher energy neutrinos. Therefore, due to the higher incident energies of the ν_μ's and ν_τ's as discussed in Section 2.1, the detector acts as a flavour filter and the supernova ν_e's contribute little to the cross section.

2.4 Neutrino Mixing Measurements

A further advantage of the detection scheme used by OMNIS is that it can independently detect mixing. If complete neutrino mixing occurs between ν_μ

and ν_e or ν_τ and ν_e, the new electron neutrino will have the higher energy of the parent mu or tau neutrino. The ν_e is the only flavour that can undergo charged current interactions:

$$\nu_e + {}^{A}_{Z}X \rightarrow e^{+} + {}^{A}_{Z}X^{*} \rightarrow {}^{A-1(2)}_{Z-1}Y + (2)n \tag{2.7}$$

Any ν_e's produced by neutrino oscillations will therefore increase the rate of charged current interactions in the detector. This section is included for completeness, as my Monte Carlo does not simulate charged current or two-neutron events. Further details may be found in [12].

2.5 OMNIS in Conjunction with Other Experiments

A full scale OMNIS detector [13] would provide an ideal complement to existing neutrino detectors, which are predominantly charged current based and therefore insensitive either to ν_μ's and ν_τ's or the flavour of the incident neutrino. Figure 2.4 illustrates this principle. Note the large signal from OMNIS for ν_μ's and ν_τ's, complementing the sensitivity of existing detectors to ν_e's.

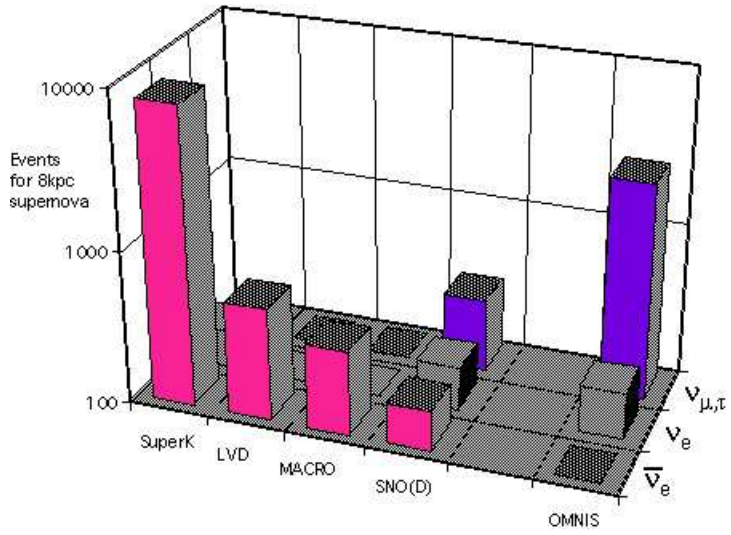

Figure 2.4: A comparison of detected neutrino events from OMNIS and other major world detectors for an 8 kpc supernova.

Chapter 3

An OMNIS Prototype Detector

3.1 The Detector

A new prototype OMNIS module design is presented in Figure 3.1. The initial dimensions of the outer layers are detailed in Table 3.1[1]. The outermost layer consists of natural lead, where the neutral current interaction occurs , followed by an air gap to allow for installation of cosmic ray counters or any further electronics. The central scintillator material consists of 4, 0.3m×0.3m×0.4m adjacent blocks of NE 102 scintillator. These are surrounded by a mixture of thermalising paraffin wax, $C_{25}H_{52}$, with natural Gadolinium powder distributed evenly within it. Light produced in the scintillator is transfered into photomultiplier tubes using light guides. An additional 0.2m air gap is present at the photomultiplier end to allow for cabling and additional electronics.

[1] The second quoted value in the third row is the percentage, by mass, of natural gadolinium powder within the wax layer. The two values in the third row of the table are the two main variables of the simulation.

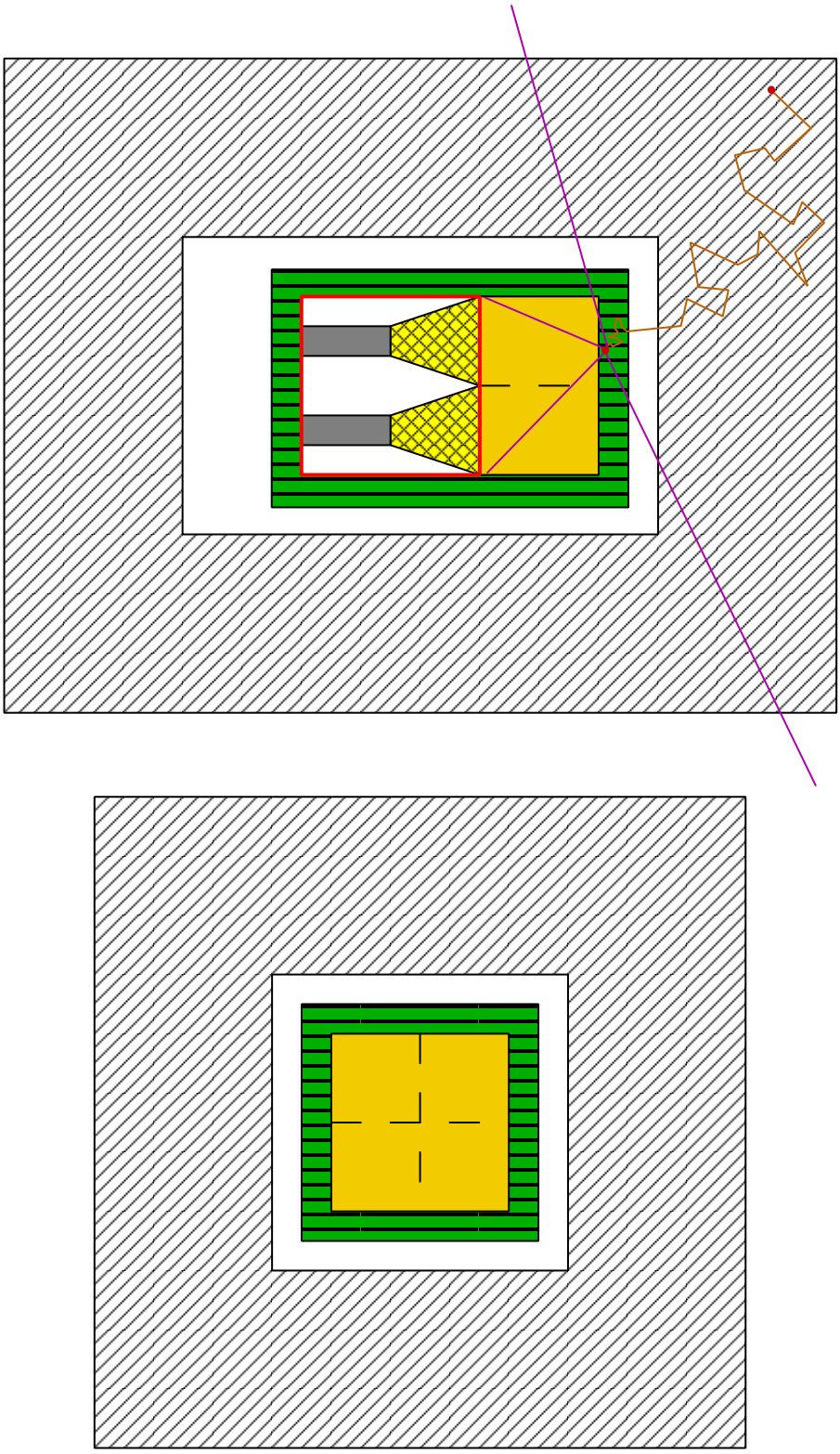

Figure 3.1: A Prototype OMNIS detector design.

Layer	Thickness (m)
Lead	0.60
Air	0.10
Wax/Gadolinium	0.10, (1.0%)

Table 3.1: The initial dimensions of the outer layers of the detector.

3.2 Modelling the Detector

The first task of my Monte Carlo is to set up a constrained 3D environment to simulate the detector. This is done so that any of the dimensions can be altered to introduce variability into the geometry of the system, although it is the thickness of the wax/Gd layer and its Gd content that are the most important parameters. The possible interactions, and their consequences are described below. Ideally, the detector needs to thermalise and capture all incident neutrons in the wax/Gd layer, whilst maximising the number of thermal neutron capture gamma decays entering the scintillator.

Several simplifying assumptions have been made about particular elements of the detector. Any neutrons entering the region to the left of the scintillator in Figure 3.1 containing the light guides and photomultipliers, hereafter referred to as the 'electronics region', are assumed lost. This is due to the complexity of modelling the region and its interactions, although the number of neutrons entering this part of the detector may be minimised, as explained in Section 4.4. Furthermore, neutrons leaving the detector's outer surface are also assumed lost. The four blocks of scintillator material are assumed to be as one. Finally, any gammas produced from thermal neutron capture are lost unless they enter the scintillator, in which case all of the energy is deposited.

Chapter 4

Modelling the Interactions

The Monte Carlo simulation begins with the production of a neutron in the lead layer of the detector. A constant initial energy of 2 MeV is assumed for all neutrons, the typical value for the neutral current interaction [9]. This implies the neutrons can be treated non-relativistically as their energy is a small fraction of their rest mass. The energy gained by the lead nucleus in the interaction is small compared to its rest mass, so the angular distribution of neutron emission is assumed to be isotropic in the lab frame.

An example of a typical event is depicted in Figure 3.1 showing the initial neutron capture, scattering, capture on a Gadolinium nucleus and subsequent decay to four gammas, of which two are shown to enter the scintillator.

4.1 Cross Section Parameterisation

Once a neutron has been produced by the neutral current inelastic scatter, it can undergo several interactions; the most significant are elastic scattering or capture on a target nucleus [14]. Both of these interactions are dependent on the energy of the incident neutron for all materials present in the detector. Therefore, the cross sections must be well modelled for the code to accurately predict the fate of a neutron in the detector. The relevant cross sections were obtained from the IAEA Nuclear Data Service [15] and modelled over the

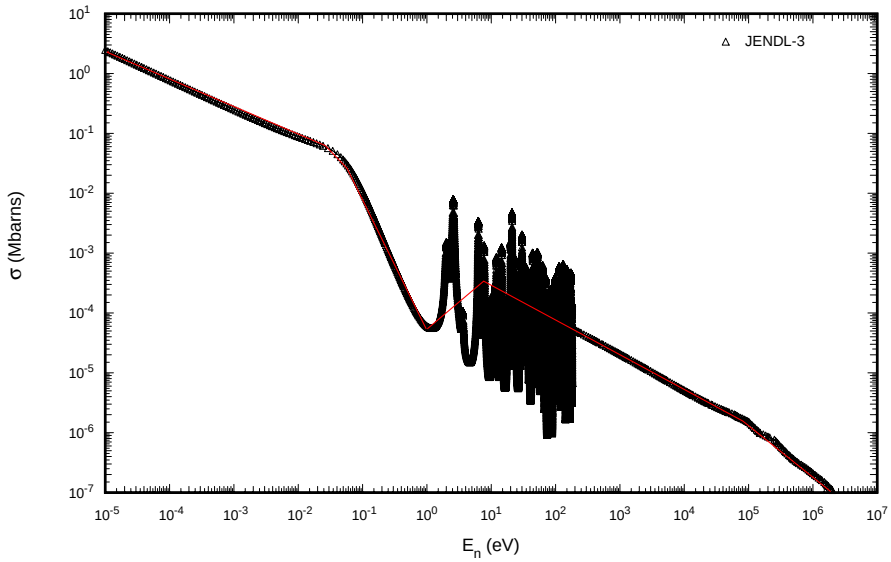

Figure 4.1: Parameterisation of the neutron capture cross section of ^{155}Gd.

relevant range of neutron energies. An example of this is displayed in Figure 4.1. Broad peaks have been parameterised but resonance peaks have been neglected. In order to model the Gadolinium decay scheme correctly, the two isotopes that contribute significantly to the total natural Gadolinium cross section have been parameterised separately. This requirement is explained in Section 4.3.

4.2 Neutron Transport

The mean number of collisions required to slow a neutron down from 2 MeV to thermal (0.025 eV) is dependent only on the atomic weight of the scattering nucleus, A, and is given by [16]:

$$\overline{N} \approx 9.1\left(A + \frac{2}{3}\right) \tag{4.1}$$

It is evident that lighter elements are more efficient scattering centres for the thermalisation of neutrons, which may be understood by considering the kinematics of the collision. A full description of this argument is given in [10]. Therefore few neutrons are likely to be thermalised in the lead layer of the detector, and hence the requirement of the hydrogenous wax layer to perform this task. The absorption of the neutrons on any nucleus in the detector is also included in the code, which in most cases is negligible until thermal energies are reached. The slowing down of neutrons via elastic scattering is effectively a problem in classical mechanics. The simplifying assumption I make is that the scattering in the neutron-nucleus centre of mass system is isotropic, which is valid for neutron energies less than a few MeV [17]. Due to the large atomic mass of the lead nuclei, scattering behaviour in the lead layer of the detector is almost identical in both frames of reference. The equations used in the Monte Carlo are detailed in Appendix A. I follow the method employed by Turner *et al.* [18], which handles a medium containing more than one type of material. This is analogous to the wax layer of the detector where 4 different target nuclei are present, so 8 different interactions are possible.

When a neutron is captured, the absorbing nucleus is left in an excited state. The subsequent decay down to ground level is assumed to be purely electromagnetic and to occur immediately. The parent nucleus may emit several gammas as it cascades back down to ground state through its energy levels. As one gamma is emitted per transition, the angular distribution of the gammas is assumed to be independent and therefore isotropic in the lab frame.

Isotope	Concentration	$\sigma_{(n,\gamma)}$ at $E_n = 0.025eV$ (barns)
^{nat}Gd	-	49700 (125)
^{152}Gd	0.2	735 (20)
^{154}Gd	2.1	85 (12)
^{155}Gd	14.8	61100 (400)
^{156}Gd	20.6	1.5 (1.2)
^{157}Gd	15.7	259000 (700)
^{158}Gd	24.8	2.2
^{160}Gd	21.8	0.77

Table 4.1: Gadolinium thermal neutron capture cross sections.

4.3 Gadolinium Interaction Modelling

4.3.1 Neutron Capture

The thermalising wax layer in the detector contains natural Gadolinium powder, to provide an efficient means of neutron absorption. Gadolinium has one of the highest capture cross sections for thermal neutrons, the details of which are displayed in Table 4.1[19]. By taking the product of the cross section and the isotope abundance, it is evident from their data that ^{155}Gd and ^{157}Gd are the dominant isotopes for absorption of thermal neutrons. The interaction is described as follows

$$^{155(157)}Gd + n \rightarrow ^{156(158)}\ Gd^{*} \rightarrow ^{156(158)}\ Gd + \gamma's \tag{4.2}$$

where the electromagnetic decay is assumed to be immediate. An s-wave capture, leading to the $J^{\pi} = 2^{-}$of the capture state, is assumed.

4.3.2 Capture γ-ray Spectra: Modelling the *Groshev* Spectrum

The energy spectrum of emitted gammas from an excited Gadolinium nucleus is extremely complicated and the most useful research carried out continues to be that done by *Groshev et al.* in the 1950's, using a magnetic Compton spectrometer. This energy spectrum is displayed in Figure 4.2 [20].

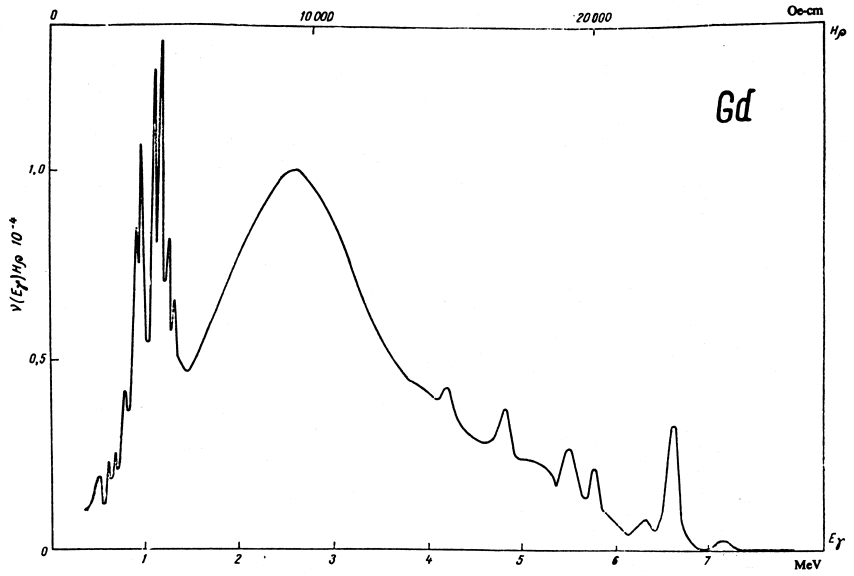

Figure 4.2: Energy spectrum of emitted gammas from $^{nat}Gd^*$, as measured by *Groshev et al.*

Previous Monte Carlo studies [10] have employed an oversimplified method of selecting gamma energies from this spectrum. This involved summing the energy of four arbitrary combinations of emitted gammas to 8 MeV, the approximate binding energy of both significant isotopes. To begin to remedy this situation, an examination of the actual decay schemes [21] of ^{156}Gd and ^{158}Gd is required. The levels below the neutron binding energy, B_n, in each of the final nuclei can be divided into two energy ranges: a discrete range and a continuum [22]. This is depicted for both isotopes in Figure 4.3, although it should be noted that $B_n(^{156}Gd) = 8.53$ MeV, whereas $B_n(^{158}Gd) = 7.93$ MeV.

Transitions from the capture level to a discrete level and between individual discrete levels by gamma emission are described on the left of Figure 4.3. These gammas appear as collections of peaks in Figure 4.2; *capture→discrete levels* at $E_\gamma \geq 4.5$ Mev, *discrete levels→discrete levels* at $E_\gamma \leq 1.5$MeV. By comparing the decay schemes as deduced by *Groshev, Bartholomew et al.* [21] of each isotope with the energies of the most intense gamma yields from

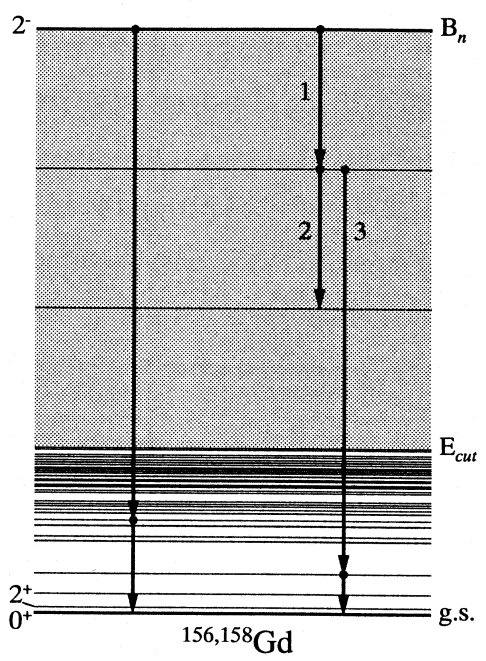

Figure 4.3: Classification of Gd γ transitions into discrete and continuum transitions.

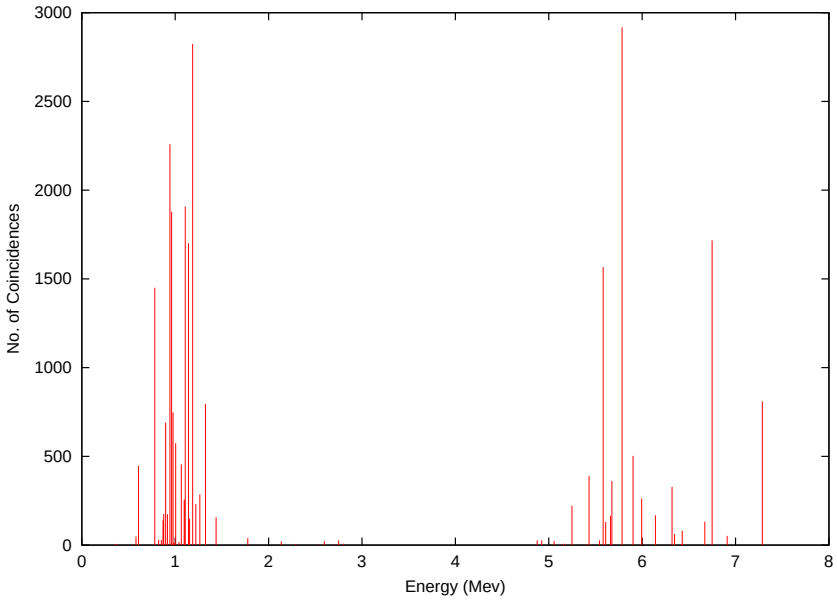

Figure 4.4: Number of coincidences of each gamma energy at perfect resolution for ^{nat}Gd for 10,000 neutron capture events.

thermal neutron capture [23], the most important decay channels of each isotope are deduced. The relative probabilities of each of these channels is found by multiplying the intensities of each constituent gamma and renormalising.

A simulation of 10,000 neutron captures on each isotope is performed, the results of which are combined using the ratio of the capture cross sections to produce an energy spectrum for ^{nat}Gd (Figure 4.4). To attempt to faithfully reproduce the Groshev spectrum and simulate the resolution of a detector, a Gaussian distribution (FWHM $= 0.02E_\gamma$) is applied to each of the lines in Figure 4.4, resulting in Figure 4.5. The heights of the Gaussians have been normalised to one.

Above a certain energy threshold, denoted E_{cut} in Figure 4.3, the detailed information about energy levels and branching ratios is unavailable. This region is the continuum range, and includes *capture state*$\rightarrow$*continuum*, *continuum*$\rightarrow$ *continuum* and *continuum*$\rightarrow$*discrete levels* transitions (labelled 1, 2 and 3 respectively in Figure 4.3). The continuum distribution is modelled using the addition of three Gaussians and is also normalised to have a

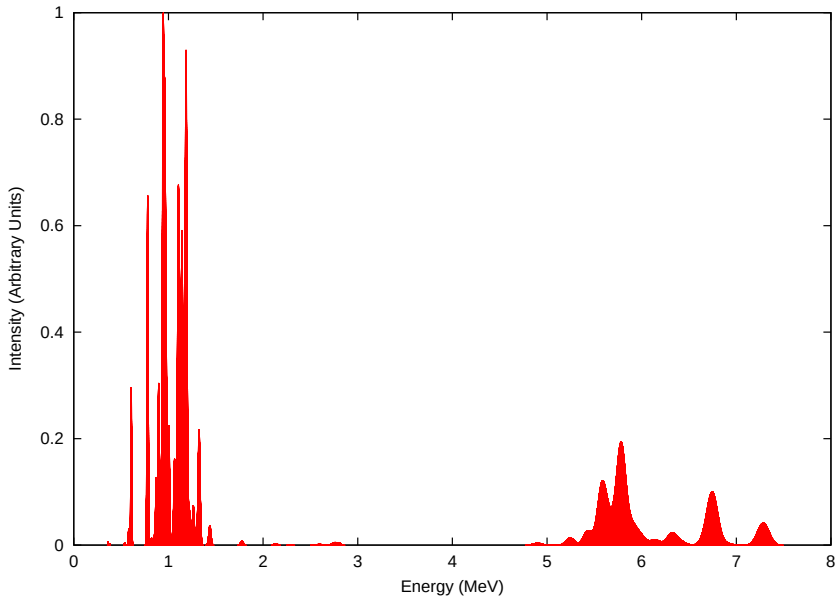

Figure 4.5: Relative intensities of gamma energies at 2% energy resolution for ^{nat}Gd.

maximum amplitude of one. The continuous part of the ^{156}Gd and ^{158}Gd spectra are almost identical, therefore this is modelled directly from the Groshev spectrum for ^{nat}Gd in Figure 4.2.

To form my energy spectrum for ^{nat}Gd decays the two components, discrete and continuum, are simply added together with the correct ratio of maximum amplitudes according to Figure 4.2. The result of this is presented in Figure 4.6.

4.3.3 Gamma Selection Methods

The Monte Carlo simulation must select gamma energies from this distribution upon neutron capture on a ^{155}Gd or ^{157}Gd nuclei in the wax layer of the detector. The ratio of the two areas corresponding to discrete or continuum emission is known, and this is the first selection process. If discrete emission is chosen, a decay channel is randomly chosen for the relevant excited nucleus, according to its probability as discussed in section 4.3.2. If

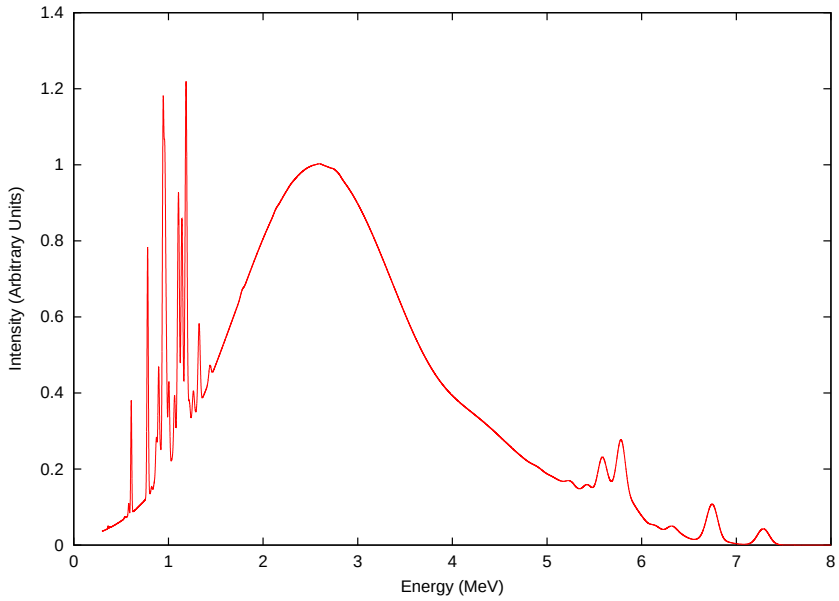

Figure 4.6: Energy spectrum of emitted gammas from $^{nat}Gd^*$, as produced by my Monte Carlo.

continuum emission is chosen, gamma energies are chosen according to the modelled continuum distribution. This is done by setting an initial energy equal to the neutron binding energy of the relevant excited nucleus and then selecting an energy from this distribution. The neutron binding energies for each isotope are slightly different and are given in the previous section. The process is then repeated, with the initial energy replaced with the energy of this gamma, until the remainder is less than 0.3 MeV. This cut off is clearly necessary, but as all of the discrete lines are above this energy it does not degrade the accuracy of the spectrum.

4.4 Other Gamma Sources

There are several background contributions to the Gadolinium gamma spectrum. Absorption of a neutron on a Hydrogen nucleus, present in the wax/Gd layer and the central scintillator, results in the emission of a single 2.22 MeV gamma as the excited nucleus returns to its ground state. However,

by maximising the efficiency of the wax/Gd layer to thermalise and capture the neutrons, the number of gammas produced in the scintillator may be minimised. This procedure will also reduce the number of neutrons entering the electronics region of the detector. Radiative capture of a neutron on a lead nuclei results in the emission of a single gamma, of energy 7.4 MeV or 6.7 MeV. Although the capture of neutrons on a Carbon nuclei is expected to be small, this possibility is also included and modelled by the code.

It has been proposed that an OMNIS detector could be installed in the Boulby mine in North Yorkshire [12]. At a depth of around 1 km below the earth's surface, background radiation from cosmic rays is vastly reduced. However, within the mine there are several natural background processes leading to gamma production. A 2.614 MeV gamma produced by thorium decay in the rock is the highest energy background source[10]. A background cut must be placed on the energy deposited in the detector of approximately 3 MeV to rule out this contribution. Therefore, we are interested in events producing a cumulative energy greater than 3 MeV of gammas entering the scintillator.

Chapter 5

Results

5.1 The Gadolinium Decay Spectrum Model

Figures 4.2 and 4.6 show a very good correlation between the spectrum generated by my Monte Carlo and that measured by *Groshev et al.* [20]. The majority of the peaks are reproduced accurately in the simulated spectrum, with the exception of the two present between 4 and 5 MeV. These peaks could be a result of dominant lines within the continuum region of the two main isotopes, for which detailed information is not known. Another possible explanation is that they represent dominant lines from other Gadolinium isotopes not included in the Monte Carlo, although this is unlikely due to their low capture cross sections (Table 4.1). The energy resolution of the detector used by *Groshev* varies non-uniformly over the range of gamma energies. This resolution is not known, and it is only approximated to produce the simulated spectrum as explained in Section 4.3.2. This is the reason for the discrepancy in the widths of the peaks between the two spectra.

The accuracy of my model of the Gadolinium decay spectrum can also be evaluated by examining the gamma multiplicity distribution for thermal neutron capture on Gadolinium. This is presented in Figure 5.1 for the initial parameters of the wax/Gd layer (given in Table 3.1), although this distribution is found to be independent of these variables. The average number of gammas produced per capture by the simulation for each isotope and for

Isotope	Average Multiplicity
^{156}Gd	4.14
^{158}Gd	3.89
^{nat}Gd	3.93

Table 5.1: Average gamma multiplicity produced for thermal neutron radiative capture in Gadolinium.

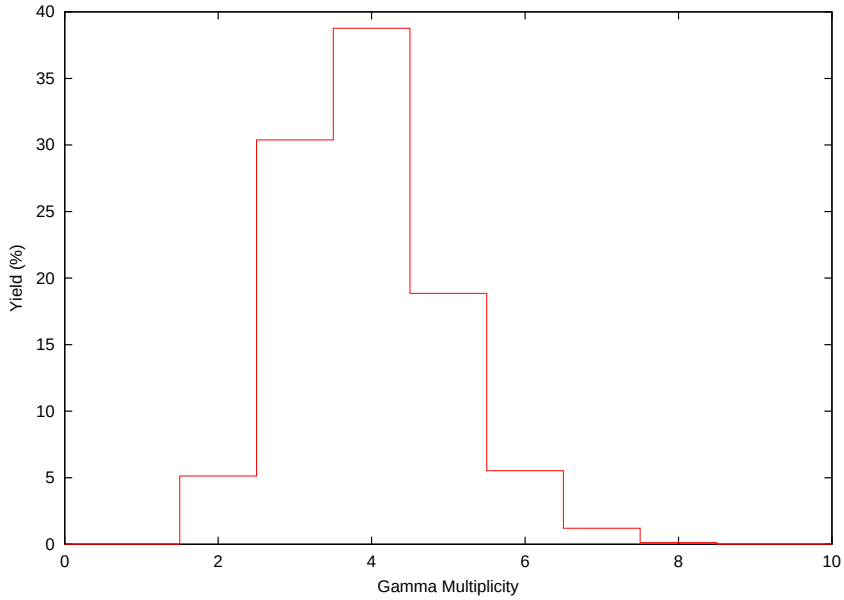

Figure 5.1: Gamma multiplicity distribution for thermal neutron radiative capture in ^{nat}Gd, as produced by my Monte Carlo.

^{nat}Gd is given in Table 5.1. These results show excellent agreement with two independent references, both of which report a measured multiplicity of 3.9 gammas per capture for ^{nat}Gd [24],[25].

5.2 The Monte Carlo Simulation

Ten thousand neutrino induced events are simulated in each run of the code. The thickness of the wax/Gd layer was varied from 1cm to 15 cm and the Gadolinium content of this layer varied from 0.1% to 2.0%, giving a total of

3 million simulated events. Other parameters and assumptions are given in previous chapters of this report.

5.2.1 Neutron Losses

Neutrons are created isotropically by the simulation in the lead layer of the detector, and subsequently scatter until they enter the central region or leave the outer surface of the detector. For this design, approximately 70% of the neutrons produced are lost outside of the detector. This number is consistent with the ratio of the areas of the inner and outer surfaces of the lead layer. Losses are reduced slightly (68%) as the wax/Gd layer thickness is increased up to 15cm, but this is a problem of the design and is analysed in the following chapter. If the thickness of the lead layer is reduced, the number of neutrons lost is also reduced, but this will consequently lower the expected number of neutral current events occurring in the detector due to neutrinos from supernovae.

As previously stated, neutrons entering the electronics region are assumed lost. The number of neutrons lost in this manner is found to be independent of the Gadolinium content of the wax/Gd layer of the detector. However, as the thickness of this layer is increased the number of neutrons entering this region rapidly decreases, as shown in Figure 5.2. The exponential behaviour of this function is expected, as the mean free path of the wax/Gd layer decreases as the number of capture nuclei within the layer increases.

5.2.2 Lead Captures

The number of lead radiative captures is approximately constant over each of the runs. About 15% of the initial number of neutrons are captured in the lead layer of the detector and of these, 4% enter the scintillator. As the energy of these gammas is greater than the proposed cut on detected events, any entering the scintillator may be included as a signal of a neutrino-nucleus interaction.

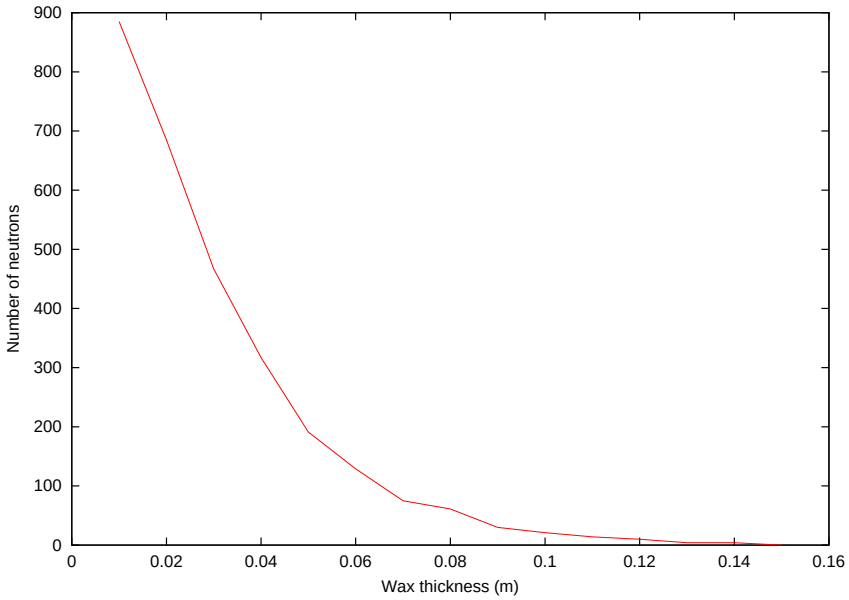

Figure 5.2: Number of neutrons lost in the electronics region of the detector for a 1.0% Gd content of the wax/Gd layer.

5.2.3 Gadolinium Captures

The number of neutron captures on either ^{155}Gd or ^{157}Gd are added together to make, in effect, the number of captures on ^{nat}Gd per run. The results for each configuration of the detector are displayed in Figure 5.3. Several trends are apparent; notably, as the thickness of the wax/Gd layer and the Gd content are increased, the number of captures also increases. However, for a given thickness the number of captures assumes an approximately constant distribution for a Gd content greater than 0.7%. Furthermore, the number of captures for a given Gd content increases much less rapidly for wax/Gd layer thicknesses greater than 7cm.

As previously stated the average number of gammas per Gadolinium capture is 3.93, produced isotropically at the point of capture. The fraction of gammas entering the scintillator is dependent only on the geometry of the detector, and not the Gd content of the wax layer. This fraction is shown for a 0.7% Gd content as a function of wax/Gd thickness in Figure 5.4. The

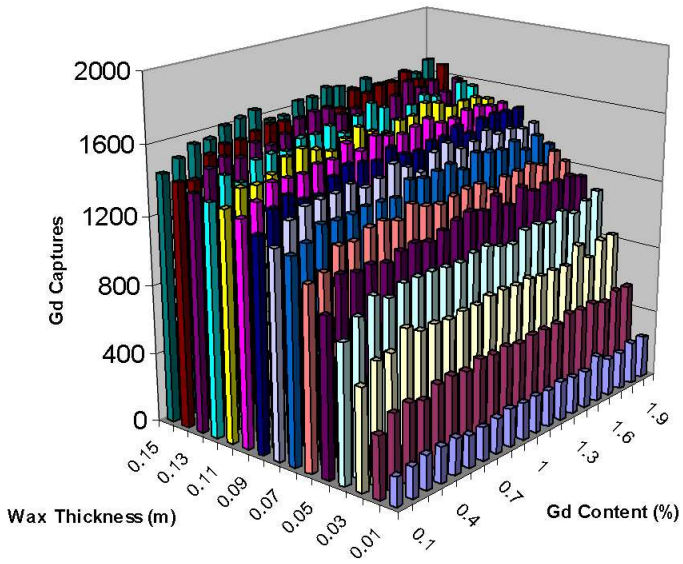

Figure 5.3: The number of thermal neutron captures on ^{nat}Gd per run for each configuration of the detector.

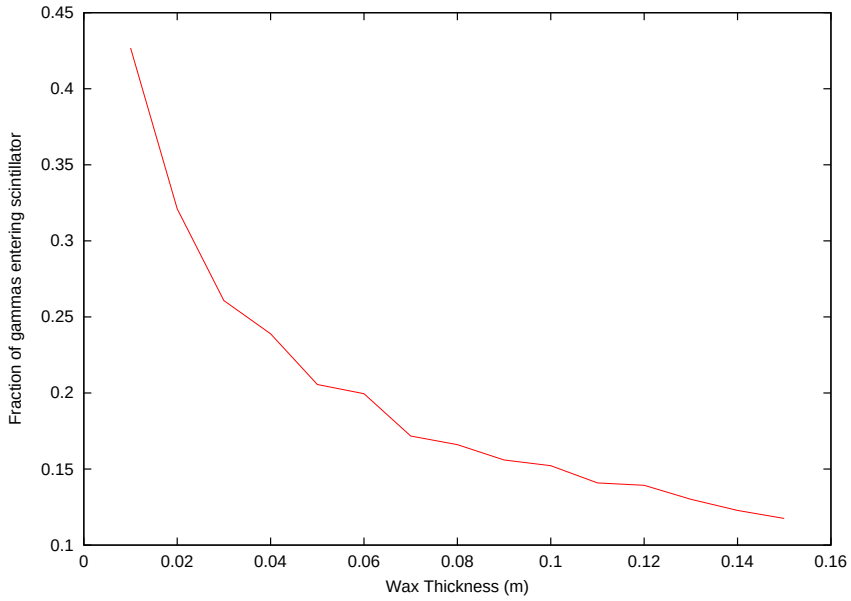

Figure 5.4: The fraction of Gadolinium gammas entering the scintillator for a 0.7% Gd content of the wax/Gd layer.

form of this function is as expected: gammas produced by captures closer to the centre of the detector have a larger solid angle projection into the scintillator. Therefore as the wax/Gd thickness is increased more captures occur further from scintillator, reducing the fraction of Gadolinium gammas entering this region of the detector.

5.2.4 Hydrogen Captures

Radiative capture of a neutron on a Hydrogen nuclei can occur on either the wax in the wax/Gd layer of the detector or within the scintillator. The occurrence of this particular interaction should be minimised as it results in the emission of a single 2.22 MeV gamma, an energy less than the proposed cut on detected events. Figure 5.5 shows the number of Hydrogen captures per run for each configuration of the detector. Note the reversed scale compared to Figure 5.3. It is immediately obvious that for smaller values of wax/Gd thickness there is a much greater number of Hydrogen captures. This is due

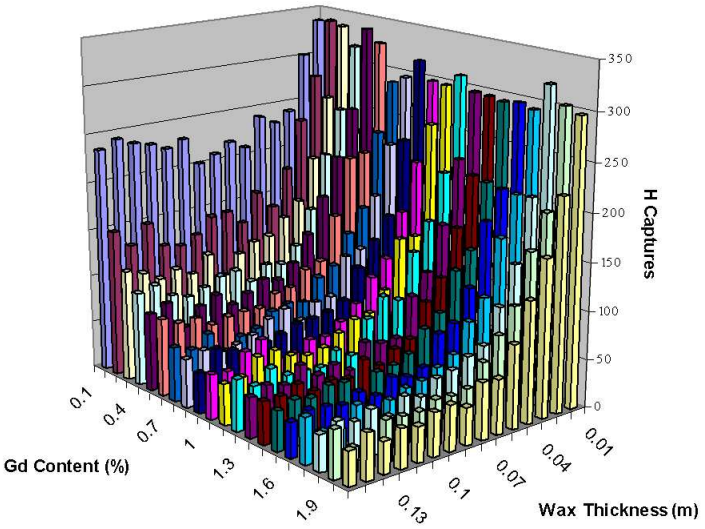

Figure 5.5: The number of thermal neutron captures on Hydrogen nuclei per run for each configuration of the detector.

to neutron capture occurring in the scintillator. When the wax/Gd thickness is increased, more neutrons are captured on Gadolinium and subsequently fewer neutrons enter the scintillator. This trend is also present for increasing Gd content. A minimum number of Hydrogen captures exists at about 7cm wax/Gd thickness and is approximately constant for a Gd content greater than 1.0%.

As the Gd content of the wax/Gd layer is increased, Hydrogen captures are more likely to occur in the scintillator from the few neutrons that reach this part of the detector, rather than in the wax/Gd layer. The fraction of Hydrogen gammas entering the scintillator (including those produced there) is subsequently found to increase with an increase of Gd/content for a particular thickness.

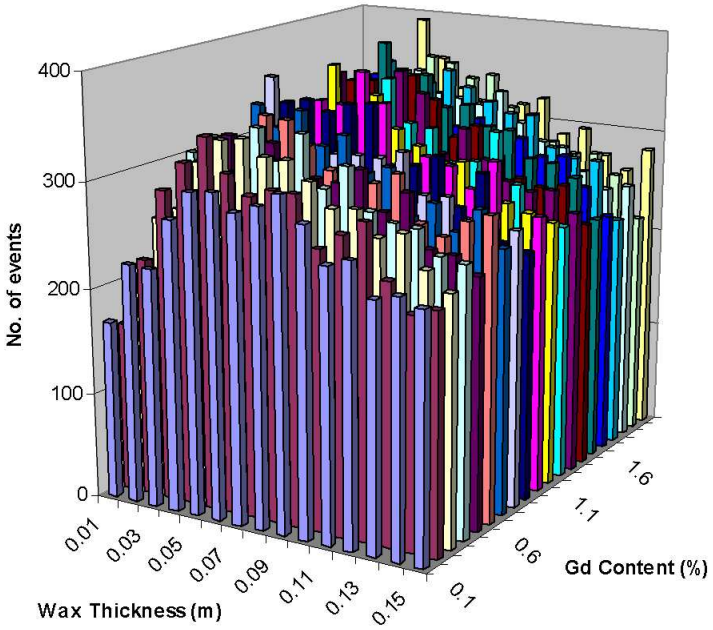

Figure 5.6: The number of events producing gammas entering the scintillator with a cumulative energy greater than 3 MeV.

5.2.5 Carbon Captures

The number of Carbon radiative captures is negligible (less than 1%) as expected, due to the low capture cross section, and tends to zero as the number of Gadolinium nuclei in the wax/Gd layer increases.

5.3 The Optimum Detector Configuration

The previous section discussed optimal parameters for specific events within the detector. To truly optimise the detector configuration, a plot of the number of events producing gammas entering the scintillator with a cumulative energy greater than 3 MeV is made (Figure 5.6). This selection process represents the number of events above the proposed background cut detailed

Event Type	Frequency
Pb captures	1540
H captures	67
C captures	0
^{155}Gd captures	237
^{157}Gd captures	1154
Lost n out of detector	6934
Lost n in electronics region	68

Table 5.2: The fate of the 10,000 neutrons in the optimal configuration simulation.

in Section 4.4. As discussed in Section 5.2.2, any gammas produced from a lead capture are included in this criteria.

For any level of Gd content, there is a clear peak in the number of desired events for a wax/Gd thickness in the range 5 to 8 cm. The optimal level of Gd content is in the range 1.0 to 1.6%. Therefore, considering this and previous discussions, optimal parameters for the detector are chosen to be a **7cm** wax/Gd layer thickness and a **1.0%** Gd content. This thickness ensures a minimum number of neutrons entering the electronics region of the detector (Fig 5.2) and a low number of Hydrogen captures (Fig 5.5). A Gd content greater than 1.0% does not significantly improve the performance of the detector.

The results from the run of 10,000 simulated neutrino-nucleus interactions for this configuration of the detector are detailed in Tables 5.2 and 5.3. Using a bin size of 0.1 MeV, the energies of the individual gammas entering the scintillator are displayed in Figure 5.7. The Hydrogen and lead gamma peaks are clearly visible, and the shape of the spectrum is consistent with the Gadolinium decay spectrum modelled. If the number of neutrons per run was increased, this similarity would be improved. The cumulative energy of any gammas entering the scintillator per event is similarly presented in Figure 5.8. A total of 728 events produce gammas that enter the scintillator, of which 330 have a cumulative energy greater than 3 MeV.

Nucleus	Total no. of gammas produced	No. entering scintillator
Pb	1540	55
H	67	30
C	0	0
^{156}Gd	975	185
^{158}Gd	4494	797

Table 5.3: Number of gammas produced by the optimal configuration simulation.

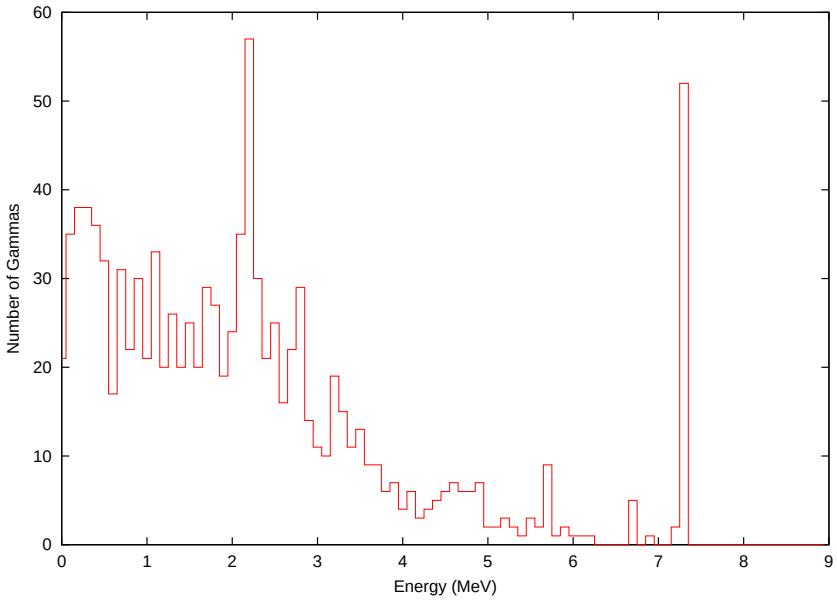

Figure 5.7: Energy of individual gammas entering the scintillator.

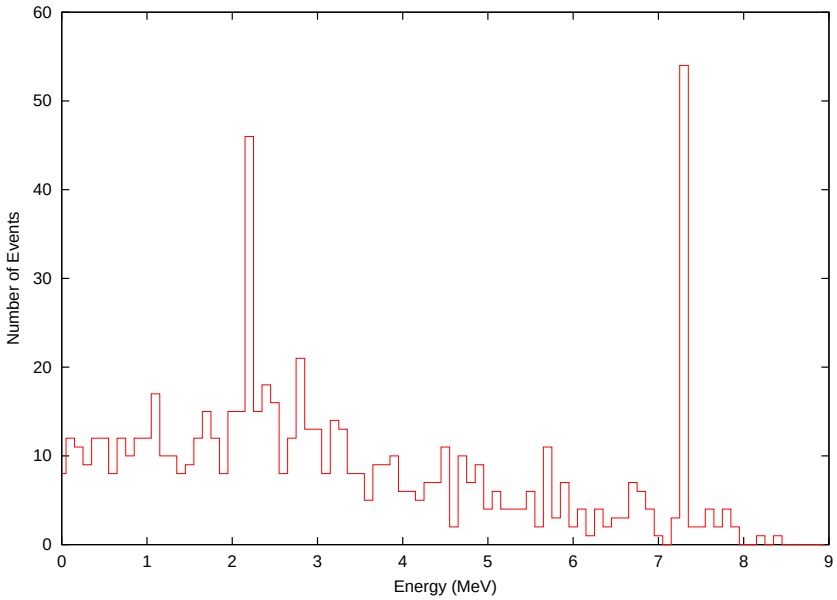

Figure 5.8: Summed energy of gammas per event entering the scintillator.

Chapter 6

Summary & Future Work

Improved parameterisation of the Gadolinium decay spectrum has enabled a more accurate simulation of the detection of neutral current interactions from supernovae neutrinos. The model presented shows very good correlation with the observed spectrum, and the energy selection method is consistent with genuine gamma decays.

As previously stated, almost 70% of the neutrons leave the detector via the outer surface of the lead layer. The detector design needs to be revised to avoid such a large number of lost neutrons. This loss may be compensated by adding an extra layer of wax/Gd outside of the lead followed by additional scintillator material. Another possible solution to this problem would be to 'turn the detector inside out' and use a lead centred detector. If the detector is to be installed in Boulby mine, reflections of neutrons off the cave walls may also be utilised.

For the optimum configuration of the detector, 330 events produce gammas entering the scintillator with a high enough cumulative energy to detect the original neutrino-nucleus interaction. However, several assumptions have been made that may in reality reduce this number. In particular, any gammas produced in the lead layer are assumed to propagate through the detector unaffected. Attenuation of gamma energy due to Compton scattering in the lead should be investigated. Any gammas entering the scintillator deposit energy via the Compton process. The maximum projected path in

the scintillator is approximately 94 cm and the mean free path of the scintillator material used is in the range 20 to 25 cm for a 2 MeV gamma. Clearly, not all gammas will deposit all of their energy within the scintillator, and this is the final part of the interaction which should be included to complete the Monte Carlo simulation.

More data is achievable from the existing code, which is approximately 3000 lines written in the C programming language. For example, for any gamma entering the scintillator the projected distance through the material is known, so including the Compton energy deposition process is easily achievable. The simulation can also be adapted to test the design modifications listed above, to attempt to minimise the number of lost neutrons.

Appendix A

Monte Carlo Equations

In all of the following equations, y is a random number between 0 and 1.

The probability that a neutron with energy, E_1 has energy $E_2 \rightarrow E_2 + dE_2$ after a collision with a nucleus, atomic number A is

$$P(E_2)dE_2 = \frac{-dE_2}{E_1(1-\alpha)} \tag{A.1}$$

where

$$\alpha = \left(\frac{(A-1)}{(A+1)}\right)^2 \tag{A.2}$$

Following standard Monte Carlo techniques, the initial and final energies are related by the following equation

$$E_2 = E_1(1 - y(1-\alpha)) \tag{A.3}$$

The probability that an interaction, an elastic scatter or absorption, occurs at a distance r in the range dr from the initial position is

$$f(r)dr = e^{-N\sigma(E)r}dr \tag{A.4}$$

where N is the number of target nuclei / m^3 and $\sigma(E)$ is the total cross section in m^2. The total macroscopic cross section, $\mu(E)$, is given by

$$\mu(E) = \sum N\sigma(E) \tag{A.5}$$

Hence,

$$r = \frac{1}{\mu(E)} \ln \frac{1}{1-y} \tag{A.6}$$

In the lead layer of the detector, for example, the probability that the neutron is scattered is given by

$$\left(\frac{N\sigma_{sc}(E)}{\mu(E)}\right)_{E=E_1} \tag{A.7}$$

Hence if y $>$ $\left(\frac{N\sigma_{sc}(E)}{\mu(E)}\right)_{E=E_1}$ then the neutron is absorbed, otherwise it is scattered.

The polar and azimuthal angles of scattering in the centre of mass frame, ξ and η, are given by

$$cos\xi = 1 - 2y \tag{A.8}$$

$$\eta = 360y \tag{A.9}$$

The corresponding angles in the lab system, ϑ and ϕ, are given by

$$cot\vartheta = \frac{M_n}{M_{Nuc}} cosec\xi + cot\xi \tag{A.10}$$

$$\phi = \eta \tag{A.11}$$

where M_n is the mass of the neutron and M_{Nuc} is the mass of the scattering nucleus.

Bibliography

[1] Dyson J. E. & Williams D. A. *"The Physics of the Interstellar Medium"*, IOP Publishing (1997).

[2] KAMIOKANDE experiment homepage; http://www-sk.icrr.u-tokyo.ac.jp/doc/kam/index.html

[3] Department of Physics & Astronomy, University of Pennsylvania; http://www.physics.upenn.edu/neutrino/jhu/node6.html

[4] Ch. Weinheimer *et al.*, Phys. Lett. D, **460**, 219 (1999).

[5] Assamagon *et al.*, Phys. Rev. D, **53**, 6065 (1996).

[6] Nikolic, I. in "International Workshop on Weak Interactions & Neutrinos", ed. G. Fiorillo, V. Palladino & P. Strolin, p.214, (Elsevier, , 1997).

[7] SUPERKAMIOKANDE experiment homepage; http://www-sk.icrr.u-tokyo.ac.jp/doc/sk/index.html

[8] The Sudbury Neutrino Observatory homepage; http://www.sno.phy.queensu.ca/

[9] Cox, B. *"Detection of Supernovae Neutrinos Using a Neutral Current Based Detector"*, 1st Year Transfer Report, May 1996.

[10] Bate, P. "*Monte Carlo Study of a Neutral Current Based Neutrino Detector"*, 1st Year Transfer Report, May 1997.

[11] Burrows, A., Phys. Rev. D, **45**, 3361 (1992).

[12] *Omnis-Siren Proposal,* Manchester, ICSTM, RAL, Sheffield and QMC.

[13] Smith, P. F., Astroparticle Physics, **8**, 27 (1997).

[14] Glasstone, S. & Edlund, M. C. *"The Elements of Nuclear Reactor Theory"*, Macmillan (1957).

[15] International Atomic Energy Agency Nuclear Data Service; http://www.iaea.or.at/programs/ri/nds/nds7.txt

[16] Kaplan I. *"Nuclear Physics"*, Adison-Wesley (1956).

[17] Cox B.E., Marshall R., Stephens K. *"The Detection of Supernova Neutrinos Using a Neutron Based Detector"*, Sheffield IOP Conference.

[18] Turner J. E. *et al.*, Health Physics, **48**, No. 6, pp. 717-733 (1985).

[19] National Institute for Standards & Technology Center for Neutron Research; http://www.ncnr.nist.gov/resources/n-lengths/elements/gd.html

[20] Groshev L. V. *et al. "Atlas of γ-ray Spectra from Radiative Capture of Thermal Neutrons"*, Pergamon Press (1958).

[21] Stephens K., University of Manchester, private communication.

[22] Trzcinski A. *et al "A Monte-Carlo Code for Neutron Efficiency Calculations for Large Volume Gd-Loaded Liquid Scintillation Detectors"*, Gesellschaft fur Schwerionenforschung mbH.

[23] Lawrence Berkeley National Laboratory; http://ie.lbl.gov/ngdata/Gd.txt

[24] The Reactor Handbook, Vol. 3, pp.46 (1962).

[25] Boehm F. *et al.*, Nuclear Instruments and Methods in Physics Research A, **300**, 395 (1991).

Acknowledgements

Thanks to my supervisor, Robin Marshall, for getting me involved in the project in the first place. Also to Keith Stephens for all his advice and ideas throughout the year and for constantly reminding me that $(mufc/nufc) > 1$. Finally, to John Levon whose expertise in C and more specifically how to debug it was much appreciated.